



HAL
open science

Functionalized geopolymer foams for cesium removal from liquid nuclear waste

S. Petlitckaia, Y. Barre, T. Piallat, O. Grauby, Daniel Ferry, A. Poulesquen

► **To cite this version:**

S. Petlitckaia, Y. Barre, T. Piallat, O. Grauby, Daniel Ferry, et al.. Functionalized geopolymer foams for cesium removal from liquid nuclear waste. *Journal of Cleaner Production*, 2020, 269, 10.1016/j.jclepro.2020.122400 . hal-02885835

HAL Id: hal-02885835

<https://hal.science/hal-02885835v1>

Submitted on 1 Jul 2020

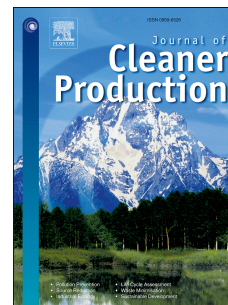
HAL is a multi-disciplinary open access archive for the deposit and dissemination of scientific research documents, whether they are published or not. The documents may come from teaching and research institutions in France or abroad, or from public or private research centers.

L'archive ouverte pluridisciplinaire **HAL**, est destinée au dépôt et à la diffusion de documents scientifiques de niveau recherche, publiés ou non, émanant des établissements d'enseignement et de recherche français ou étrangers, des laboratoires publics ou privés.

Journal Pre-proof

Functionalized geopolymer foams for cesium removal from liquid nuclear waste

S. Petlitchkaia, Y. Barré, T. Pierrat, O. Grauby, D. Ferry, A. Poulesquen



PII: S0959-6526(20)32447-1

DOI: <https://doi.org/10.1016/j.jclepro.2020.122400>

Reference: JCLP 122400

To appear in: *Journal of Cleaner Production*

Received Date: 18 February 2020

Revised Date: 25 April 2020

Accepted Date: 18 May 2020

Please cite this article as: Petlitchkaia S, Barré Y, Pierrat T, Grauby O, Ferry D, Poulesquen A, Functionalized geopolymer foams for cesium removal from liquid nuclear waste, *Journal of Cleaner Production* (2020), doi: <https://doi.org/10.1016/j.jclepro.2020.122400>.

This is a PDF file of an article that has undergone enhancements after acceptance, such as the addition of a cover page and metadata, and formatting for readability, but it is not yet the definitive version of record. This version will undergo additional copyediting, typesetting and review before it is published in its final form, but we are providing this version to give early visibility of the article. Please note that, during the production process, errors may be discovered which could affect the content, and all legal disclaimers that apply to the journal pertain.

© 2020 Published by Elsevier Ltd.

Svetlana Petlitckaia : Methodology, Investigation

Yves Barré : Investigation, Methodology

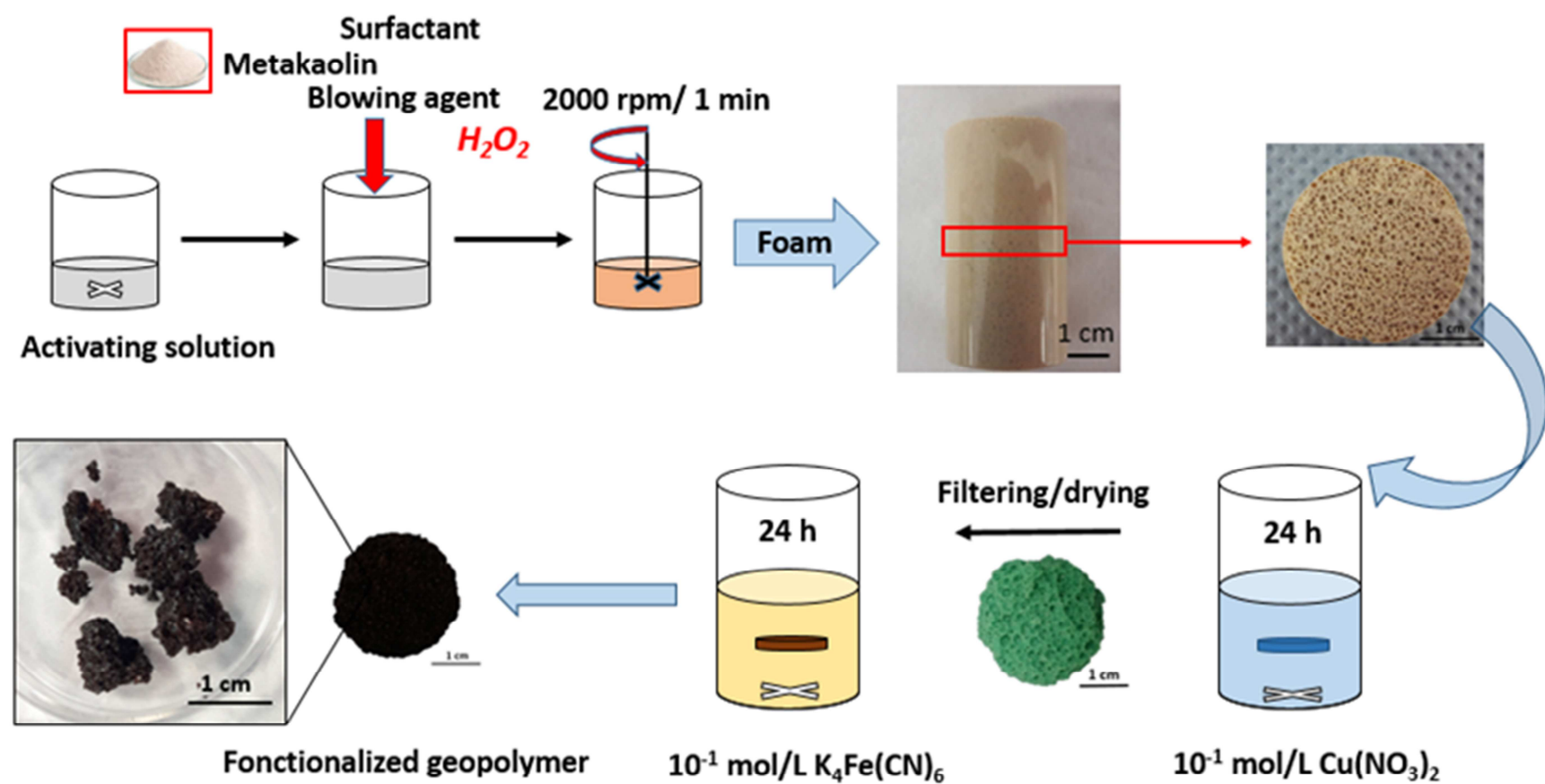
Thomas Piallat: Investigation

Olivier Grauby: Investigation

Daniel Ferry: Investigation, Writing – Original draft

Arnaud Poulesquen : Supervision, Writing – Review & Editing

Journal Pre-proof



Functionalized geopolymer foams for cesium removal from liquid nuclear waste

S. Petlitckaia^(a), Y. Barré^(b), T. Piallat^(a), O. Grauby^(c), D. Ferry^(c), A. Poulesquen^{(a)*}

(a) CEA, DES, ISEC, DE2D, SEAD, LCBC, Univ Montpellier, Marcoule, France

(b) CEA, DES, ISEC, DE2D, SEAD, LPSD, Univ Montpellier, Marcoule, France

(c) Aix Marseille Univ, CNRS, CINaM, F-13009 Marseille, France

*Corresponding author arnaud.poulesquen@cea.fr

Keyword: Functionalized geopolymer foam, Cesium uptake, selectivity, competitive ions, ion exchange

Abstract

Geopolymer foam hosting a 3D network of interconnected pores was synthesized and functionalized with a potassium copper hexacyanoferrate $[\text{K}_2\text{CuFe}(\text{CN})_6]$ in order to decontaminate radioactive liquid waste containing cesium. The Geopolymer Foam (GF) and Functionalized Geopolymer Foams (FGF) were characterized using a panel of characterization techniques (SEM, TEM, XRD...) before studying their capacity to remove selectively cesium from the solution. $\text{K}_2\text{CuFe}(\text{CN})_6$ homogeneously precipitates on the pore walls of the foam and into the mesoporous network. Exploiting kinetic and adsorption isotherms in various solutions (deionized water, fresh water and fresh water with excess of sodium), a comparative study between the GF and FGF was undertaken. In presence of competitive ions into the solution, the capacity of both materials decreases with respect to the deionized water. The mechanism of exchange is $\text{Na}^+ \leftrightarrow \text{Cs}^+$ and $\text{K}^+ \leftrightarrow \text{Cs}^+$ for GF and FGF

respectively. Although the GF material presents some very high performances in term of ion exchange, in excess of sodium ions, the GF material completely loses its capacity with respect to the FGF that remains constant up to 1 mol/l^{-1} . FGF is therefore very selective with regard to the cesium if other cations coexist into the solution. This is also confirmed by experiments performed in radioactive environment for very low concentration of radioactive cesium where the distribution coefficient (K_d) for the FGF reaches in average $3.5 \cdot 10^5 \text{ ml.g}^{-1}$ that is ten times higher than for the GF material.

1. Introduction

The nuclear industry generates volumes of radioactive effluents containing Cs. They have to be treated to minimize both their volume and environmental impact. Nine years after the Fukushima nuclear reactor disaster in Japan, a huge quantity of aqueous radioactive waste containing fission products and actinides still remains and has to be treated and safely stored in a confinement matrix (Lehto et al., 2019; Thakur et al., 2013). Various solutions such as membrane process, coagulation, electrochemical, co-precipitation, ion exchange and adsorption were proposed to clean and reduce the volume of contaminated effluents (Chen and Wang, 2008; Park et al., 2010; Sheha and Metwally, 2007; Sun et al., 2012; Vincent et al., 2015). One of the most common and efficient processes for selectively trapping radioelements is the ion exchange in a fixed-bed column. Various clays such as montmorillonite, illite as well as natural zeolites can also carry out this trapping (Johan et al., 2015; Staunton and Roubaud, 1997). However, the good adsorption capacity of Cs drastically drops in high saline water or in presence of Na^+ , K^+ , Mg^{2+} or Ca^{2+} competitive ions in the solution. The high selectivity for trapping cesium is the key point in order to collect traces of radioactive Cs from seawater for instance. Specific colloidal adsorbents of cesium like metal potassium hexacyanoferrates enable selective Cs exchange. They are known as Prussian Blue Analogues (PBA) and exhibit a great variety of compositions and structures (Vincent et al., 2014). For

example, fixation of cesium on copper – potassium hexacyanoferrate $K_2CuFe(CN)_6$ has already been reported (Ayrault et al., 1998; Loos-Neskovic et al., 2004). In this case, ion exchanges take place between potassium from the solid and cesium in solution. This material presents a high ability to trap the cesium ions over a wide range of pH and salinity due to a selective insertion of Cs^+ into the crystalline structure (Haas, 1993; Lehto et al., 1987; Loos-Neskovic et al., 2004; Parajuli et al., 2016). The use of $K_2CuFe(CN)_6$ at colloidal state in the column process is, however, limited due to its poor mechanical properties that lead to clogging problems (Delchet et al., 2012) in dynamical processes. For this reason, it is necessary to immobilize these particles in porous solid matrices of micrometric size in order to limit the pressure loss during the treatment (Michel et al., 2017, 2015). All powdered mineral adsorbents that are used in column need to be stabilized, confined and therefore conditioned in an inorganic matrix like cement for example. In order to avoid the use of mineral exchangers in a powder form, studies focus on the development of a monolithic material with high mechanical resistance and tailored macroporosity. Such a material has the double advantage of continuously decontaminating liquid effluents (open macroporosity and low sensitivity to pH and salt water) and of being considered as an ultimate waste (good mechanical and radiation resistance).

The use of geopolymer foams has a real potential for the decontamination of liquid nuclear waste. Geopolymers are three-dimensional aluminosilicate binder materials that can be produced at ambient temperature by alkaline activation of aluminosilicate sources (Duxson et al., 2007). This material has an amorphous structure containing tetrahedrally coordinated aluminum and silicon atoms. The deficit of the charge balance of tetrahedral Al is compensated by the presence of alkali such as Na^+ , K^+ (Barbosa and MacKenzie, 2003; Benavent et al., 2016b; Luukkonen et al., 2016; O'Connor et al., 2010; Skorina, 2014; Steins et al., 2012). Consequently, geopolymer can be viewed as an amorphous analogue of a zeolite

capable of cations exchange (Bortnovsky et al., 2008; Sazama et al., 2011). The interest in geopolymers stems from their high compressive strength, good chemical and thermal resistance and good ageing properties and durability, which are beneficial for a number of industrial applications [27]–[29]. Using geopolymer monolith, granules and powders for extraction of heavy metal, methylene bleu and cesium have already been reported (Al-Zboon et al., 2011; El-Naggar and Amin, 2018; Liu et al., 2016; Novais et al., 2018, 2016) but the use of selective sorbent towards cesium grafted onto geopolymer monolith has never been discussed.

The main objective of this study is to use lightweight geopolymer monoliths with a hierarchical connected pores network as a solid support for grafting copper -potassium hexacyanoferrate into the porous network. The ability of these hybrid materials to selectively trap cesium was assessed in both radioactive and non-radioactive environment and compared to the trapping capacity of the non-functionalized geopolymer foam. We therefore studied the effect of functionalization and the presence of competitive ions in the solution on the ability to selectively decontaminate some radioactive effluents containing Cs.

2. Experimental conditions

2.1 Materials

Commercial sodium silicate solution (Woellner, Betol® 39T: 27.8 % SiO₂, 8.3 % Na₂O and H₂O 63.9 %), sodium hydroxide (99 %, Sigma Aldrich) and alumino-silicate source (metakaolin, ARGICAL-M 1000) were used to synthesize geopolymer foams. Hydrogen peroxide (density = 1.19 g.cm⁻³ and M = 34.015 g.mol⁻¹) with a concentration of 50 % w/w was used as chemical foaming agent and obtained from Sigma-Aldrich. A commercial air entraining Sika®AER5 was used as surfactant to stabilize air bubbles and the homogeneity

of the synthesized geopolymer foam. Copper Nitrate ($\text{Cu}(\text{NO}_3)_2$) and potassium hexacyanoferrate ($\text{K}_4\text{Fe}(\text{CN})_6$), purchased from Sigma-Aldrich were used as precursors to functionalize geopolymer foams with copper hexacyanoferrate. Inactive cesium nitrate provided by Sigma-Aldrich was used for the majority of adsorption tests and radioactive ^{137}Cs and ^{133}Cs were also used and handled in a glove box to assess the ability of the hybrid geopolymer to trap radioactive traces of cesium.

2.2 Geopolymer adsorbant preparation

Geopolymer foams were synthesized with the molar composition $\text{SiO}_2/\text{Al}_2\text{O}_3/\text{Na}_2\text{O}/\text{H}_2\text{O} = 3.6/1/1/12$. Hydrogen peroxide was added at concentrations $R = 1.25\%$ v/v (R being the ratio between the initial volume of H_2O_2 , $V_{\text{H}_2\text{O}_2}$, and the initial volume of geopolymer paste, V_0). The main characteristics and the procedure of production of the geopolymer foam are detailed elsewhere (Petlitchkaia and Poulesquen, 2019).

After consolidation, the geopolymer foam was immersed into an aqueous solution of 10^{-1} mol/L of $\text{Cu}(\text{NO}_3)_2$ under mild stirring for 24 h. The color of geopolymer foam changes into green. The sample was washed three times with deionized water. Then the foam was placed into solution of 10^{-1} mol/L $\text{K}_4\text{Fe}(\text{CN})_6$ also for 24 h under mild stirring. After the second step of functionalization, the material turned brown. This functionalized Geopolymer Foam (FGF) was washed three times with deionized water and then filtered. The different steps of preparation are detailed in Figure 1.

2.3 Characterization techniques

X-Ray Diffraction (XRD) measurements were carried out using a device mounted on a high-gloss rotating copper anode, Rigaku RU-200BH. A reflective focusing optics, OSMIC, mainly transmits the Cu K α radiation ($\lambda = 1.5418\text{\AA}$) and a very small part of the K β , the latter being completely absorbed by a Ni filter. A 2D detector, flat image type, model Mar345 is used. XRD patterns were collected from quartz capillaries containing crushed samples and experimental settings were a working power of 50 kV, an intensity of 50 mA and a beam size of $0.5 \times 0.5 \text{ mm}^2$.

Low and high-resolution micrographs of samples were recorded with a scanning electron microscope (SEM) JEOL JSM-6340F at an acceleration voltage of 15keV. Samples were crushed, glued on a carbon tape and then coated with a thin carbon layer prior to any SEM imaging.

Energy Dispersive X-Ray (EDX) microanalyses of samples were conducted using a X-Flash Silicon Drift Detector 5030 (Bruker) that equips a JEOL JEM 2011 Transmission Electron Microscope (TEM). Data collection parameters were set as follows: TEM magnification of 50 000 x, 4L spot size, angular tilt of 20° toward the EDX detector, time constant of 60 kcp.s^{-1} , energy range of 40 keV, and a corrected counting time of 30 seconds. The electron beam diameter was set to $\sim 20 \text{ nm}$ (200\AA) and EDX spectra were recorded from suspensions of crushed samples in water that were deposited on carbon-coated nickel grids and air dried.

Measurement of specific surface area, pore volume, and pore size distributions were carried out in a Micrometrics ASAP 2020 instrument by N $_2$ adsorption/desorption at 77K. Geopolymer samples without functionalization were frozen – dried with liquid nitrogen for

96 h before being outgassed under vacuum at 90 °C for 120 min and then heated up to 350 °C for 600 min. Functionalized geopolymer foams was outgassed under vacuum at 80 °C for two days prior to analysis. The specific surface area was determined from the Brunauer-Emmet-Teller (BET) method. The isotherm's desorption branch was used to establish the pore size distribution from the Barret-Joyner-Halenda (BJH) model, which assumes a cylindrical pore geometry. Pore volumes were calculated from the amount of adsorbed nitrogen at the relative pressure P/P^0 of 0.99.

The concentration of cation in aqueous solution from non-*radioactive* batch sorption experiments were analyzed by Atomic Adsorption Spectrometry (AAS) with a PERKIN ELMER spectrometer and inductively-coupled plasma atomic emission spectroscopy (ICP-AES Thermo Scientific). Radiochemical analyses of residual ^{137}Cs in the doped solution were performed by gamma counting (Eurisy, measured with a germanium detector).

2.4 Sorption experiment

Sorption experiments were carried out in batch mode using a rotating agitator by immersing the geopolymer foams in solution. The capacity of ion exchange for all experiments was calculated by the following equation 1:

$$Q = (C - C_0) * \frac{V}{m} \quad (1)$$

where Q (mg/g) is the Cs exchange capacity, C_0 (mg/l) is the initial concentration in the solution, C (mg/l) is the equilibrium concentration, V (l) is the volume of material and m (g) its mass.

The following equations were used to assess and compare the materials performance:

$$K_{d,Cs} = \frac{(C_0 - C)}{C} * \frac{V}{m} = \frac{Q}{C} \quad \text{or} \quad K_{d,Cs} = \frac{(A_i - A_f)}{A_f} * \frac{V}{m} \quad (2)$$

where K_d (ml/g) is the distribution coefficient, $(C_0 - C)$ (mol/g) the concentration captured by the solid, C (mol/l) the equilibrium concentration in the solution, A_i – the initial activity (Bq/l), and A_f is the activity at equilibrium (Bq/l).

Finally, the decontamination factor DF of samples can also be evaluated and is defined by the ratio:

$$DF = \frac{A_i}{A_f} \quad (3)$$

Kinetic experiment

One gram of monolithic adsorbent was immersed in one liter of solution (deionized water) containing 100 ppm of Cs^+ ($7.52 * 10^{-4}$ mol/l) and stirred during 24 h. Aliquots were taken from this solution at different time intervals, namely 5, 10, 20, 40, 60, 120, 240, 360 and 1440 minutes. Each sample was filtered by a 2 μm syringe filter and analyzed by Atomic Adsorption Spectrometry (AAS). This experiment enabled us to determine the time required to reach equilibrium. The kinetic experiment was performed for both the geopolymer foams (GF) and functionalized geopolymer foams (FGF).

Isotherm of adsorption

In this work, experiments to assess the FGF potentiality to selectively trap Cs were conducted over a wide range of cesium concentrations. Indeed, a set of adsorption experiments was performed in deionized water (DW) and in fresh water (FW) for both

materials (GF and FGF). The use of fresh water whose composition is given in Table 1 allows to determine the maximum capacity of both materials to trap cesium in presence of competitive ions. Another set of experiments consists in assessing the selectivity of both materials by increasing the sodium concentration in the fresh water.

For all the sorption experiments presented in this paper, 50 mg of material were placed in 50 ml of solutions (DW or FW) doped with different concentration of Cs^+ ranging from 30 to 1000 ppm ($[2.26 \cdot 10^{-4} - 7.52 \cdot 10^{-3} \text{ mol/l}]$). For the isotherm with a constant cesium concentration of $[\text{Cs}^+] = 50 \text{ ppm}$ ($3.76 \cdot 10^{-4} \text{ mol/l}$ in fresh water), the concentration of NaNO_3 was swept between 0.01 and 1 mol/l. For all experiments, after 24 h of contact time insuring to reach the maximum capacity, the solid and liquid phases were filtered by using a 2 μm syringe and analyzed by AAS and ICP.

Isotherms in radioactive conditions were performed in fresh water (FW) containing ^{137}Cs with an initial activity of 54 kBq/l ($1.22 \cdot 10^{-10} \text{ mol/l}$) and two solutions having respective ^{133}Cs concentrations of $1.5 \cdot 10^{-5}$ and $1.5 \cdot 10^{-8} \text{ mol/l}$ with an initial activity of 40 kBq/l. For these experiments in radioactive environment, 50 mg of adsorbent were placed for 24h into 50 ml of solution and traces of radioactive cesium were measured by gamma counting.

3. Results and discussion

3.1 Characterization of adsorbents (GF and FGF)

Scanning Electron Microscopy (SEM) images recorded at various magnifications show the microstructure of the functionalized geopolymer foam (FGF) in **Figure 2**. Platelet shaped particles cover homogeneously the geopolymer walls but their size distribution seems very spread out. It is clearly visible in SEM images recorded at low (fig. 2-c) and high (fig. 2-f) magnifications where precipitates have respective average sizes of 3 μm and less than 1 μm (Loos-Neskovic et al., 2004; Vincent et al., 2014). The multiscale porous network of

geopolymer foams likely plays a role on the precipitates size through confinement effects. **Figure 2b** and **2d** exhibit particles that seem closely linked to the solid but the origin of these strong interactions is not fully understood to date. Nevertheless, Benavent et al (Benavent et al., 2016a) have shown that the interstitial solution of the geopolymer is very basic with a pH value of about 13 and then copper in contact with the interstitial solution precipitates on the pore walls to form the Rouaite phase (see XRD pattern in **Figure 5**). $K_2CuFe(CN)_6$ therefore grow from the latter copper precipitates strongly attached to the pore wall (Abousahl et al., 1994). Liu et al (Liu et al., 2016) also report that $K_4Fe(CN)_6$ has an affinity to coordinate with aluminum atoms available at the geopolymer surface. But, as already mentioned, the functionalized materials were washed three times after the synthesis and none of these particles were detected in the leachate. Note that we do not attempt here to optimize the size of the precipitates with different operating conditions but we are however fully aware that this is a key parameter for both the uptake kinetics and sorption isotherm as discussed by Vincent et al in their Mini-Review (Vincent et al., 2015). The geopolymer foam has a multiscale porous network made of both macropores (created by the H_2O_2) and intrinsic mesopores resulting from the geopolymerisation reaction (Petlitzkaia and Poulesquen, 2019). Therefore, high-resolution TEM imaging was performed to visualize the mesoporous network before and after functionalization. **Error! Reference source not found.** shows that some particles precipitates into mesopores and likely prevent access to the mesoporous network. This is confirmed by the nitrogen adsorption-desorption isotherm shown in **Figure 4**, where the quantity adsorbed and specific surface area drastically drop from $130\text{ cm}^3.\text{g}^{-1}$ to $55\text{ cm}^3.\text{g}^{-1}$ and from $69\text{ m}^2.\text{g}^{-1}$ to $35\text{ m}^2.\text{g}^{-1}$ respectively. The pore size distribution is affected by the precipitation of particles since the mesopore mean size increases and the accessible pore volume decreases (Figure S1 in Supporting Information file). Another way to validate the presence of nanoparticles into the mesoporous network consists in probing the interface

between the solid framework of geopolymer and the pores by using Small Angle X-Ray Scattering (SAXS). A modification of the interface at the nanoscale is observed after the materials functionalization (Figure S2 in SI). All of these results from various experimental techniques enable us to assume that nanoparticles are embedded in the mesoporous network.

The geopolymer foam is classically made of Quartz and traces of Anatase and Illite (impurities of the metakaolin). GF and FGF samples were analysed by X-ray powder diffraction and spectra in **Figure 5** show the well-known amorphous bump of geopolymers centered on $2\theta = 28-29^\circ$. Additional peaks corresponding to the Rouaite phase ($\text{Cu}_2(\text{NO}_3)(\text{OH})_3$) and the potassium copper hexacyanoferrate ($\text{K}_2\text{Cu}(\text{Fe}(\text{CN})_6)$) crystallized in cubic and tetragonal phases (cf. the raw X-ray diffraction pattern without subtraction given in Figure S3 in SI) appear on the XRD pattern after functionalization. The Rouaite phase, which is responsible for the green color after the first step of impregnation as shown in **Figure 1**, turns to brown when the $\text{K}_2\text{Cu}(\text{Fe}(\text{CN})_6)$ grow from the Rouaite precipitates. This characterization confirms the presence of K, Cu, and Fe in the geopolymer after the two cycles of impregnation, as also evidenced from EDX measurements (cf. figure 3b).

3.2 Sorption of cesium on adsorbents

3.2.1 Uptake kinetics

Cesium sorption kinetics of over 24 hours are reported in **Figure 6**. Kinetics are similar for both materials (GF and FGF) and the equilibrium is reached after 4-5 hours. The maximal exchange capacity is about $80 \text{ mg}\cdot\text{g}^{-1}$ for GF and $65 \text{ mg}\cdot\text{g}^{-1}$ for FGF and the difference in their adsorption capacity is explained by the excess of cation Na^+ in the GF structure that participate to the ion exchange. Indeed, as previously mentioned, the synthesis of FGF sample implies two steps of impregnation and several steps of washing by pure water. These steps

entail a deficit of sodium in the FGF with respect to the GF that has neither undergone these steps. The total concentration of alkali cations (K^+ and Na^+ released in solution and Cs^+ sorbed on the foams) was measured in order to understand the ion exchange mechanism and compare for the two samples. Regarding the GF sample, cesium is exclusively exchanged with sodium that acts as a charge compensator of aluminum in the geopolymer matrix whereas for the FGF the cesium is exchanged with potassium (see Figure S4 in SI), which fills in the center of small cubes in the $CuFe(CN)_6$ unit cell. The concentration of cations at the equilibrium are given in Table 2, which shows that sodium concentrations released into the solution are two order of magnitude higher for the GF than the FGF whereas cesium uptake by both materials is approximately the same. Table 2 also gives ratio values between exchangeable cations and a value close to 1 is obtained between potassium and cesium for FGF.

3.2.2 Sorption isotherms

Sorption isotherms in absence and in presence of competitive ions are reported in Figure 7-a and -b respectively. They allow us to determine sorption capacities of GF and FGF that are respectively equal to 250 mg.g^{-1} and 175 mg.g^{-1} in pure water. Equilibrium plateaus were reached for a minimal aqueous Cs concentration of $2.8 \cdot 10^{-3} \text{ mol.l}^{-1}$ for the both adsorbents and a decrease of the sorption capacity that appear beyond $[Cs^+]_{eq} = 3.92 \cdot 10^{-3} \text{ mol.l}^{-1}$ for the GF adsorbent can be explain by the saturation of active exchange sites of the material (cf. Figure 7-a). The exchange capacity of the GF sample is higher than the one of FGF sample for the same reasons, namely the initial concentration of sodium is 100 times higher (see Figure S5 in SI). The concentration of cesium trapped onto the solid is approximately the same for both foams but $Na^+ \leftrightarrow Cs^+$ exchanges occur in GF whereas $K^+ \leftrightarrow Cs^+$ exchanges occur in FGF, as shown in Figure S5. Cation ratio and concentrations at equilibrium are given in Table 3.

In fresh water, the exchange capacity at equilibrium decreases due to presence of competitive cations (K^+ , Na^+ , Mg^{2+} , Ca^{+2}) which prevent or limit the access of cesium to the exchange sites, Figure 7-b. The sorption capacity is about 150 mg.g^{-1} and 100 mg.g^{-1} for GF and FGF respectively. Ions exchange process is the same than already discussed and concentration of ions are reported in Figure S6. Table 4 gathers the concentration at equilibrium and the ratio between the main exchangeable cations.

In order to check the selectivity of both foams with regard to the cesium, two sets of experiments were conducted. The first one consists in a sequential addition of sodium in fresh water. As shown in **Figure 8**, the geopolymer foam quickly loses his selectivity when the concentration of sodium increases. At a concentration of 0.5 mol.l^{-1} (concentration of seawater), the GF exchange capacity is seven times lower than those of FGF and reaches zero at 1 mol.l^{-1} . FGF is therefore very selective for cesium removal due to the presence of the $K_2Cu(Fe(CN)_6)$ while GF is not.

The second experiment consists in using some radioactive ^{137}Cs and ^{133}Cs at very low concentrations to determine the distribution coefficient (K_d). As shown in **Figure 9**, K_d is constant at trace concentration of Cs for both samples, up to approximately $10^{-5} \text{ mol.l}^{-1}$, and then linearly decreases (in logarithmic scale) with increasing Cs concentration. K_d is ten times higher for the FGF sample than for the GF one with respective mean values of $3.5 \cdot 10^5 \text{ ml.g}^{-1}$ and $3.8 \cdot 10^4 \text{ ml.g}^{-1}$. Note that these values are in the same order of magnitude than those recently reported in (Grandjean et al., 2020). The decontamination factor (DF) is ranged from 245 to 667 for the FGF and from 25 to 56 for the GF.

For performance point of view, it means that the FGF can treat in average 350 l.g^{-1} of contaminated liquid waste with a very high selectivity even in presence of competitive ions and for some traces of Cs.

4. Conclusion

This paper investigated the potentiality of a geopolymer foam (GF) or a functionalized geopolymer foam (FGF) to selectively remove cesium from radioactive liquid effluent. The geopolymer foam was formulated to have a 3D network of interconnected pores in order to facilitate the mass transfer of fluid through the materials. Potassium copper hexacyanoferrate ($K_2CuFe(CN)_6$), chosen for its capacity to selectively trap cesium by an ion exchange process, was synthesized in-situ by two successive steps of impregnation. $K_2CuFe(CN)_6$ homogeneously precipitates on the pore walls of the foam and into the mesoporous network. A comparative study between the GF and FGF was undertaken in term of exchange capacity and distribution coefficient from kinetic and adsorption point of view. Both materials reach the equilibrium in 4-5 hours and show a very high capacity to uptake cesium from the solution. The capacity at equilibrium of the GF is always higher than that of FGF due to the initial excess of sodium. In presence of competitive ions (fresh water), the exchange capacity decreases for both foams. Whatever the composition of the solution, a $Na^+ \leftrightarrow Cs^+$ exchange mechanism takes place for the GF sample whereas an exchange $K^+ \leftrightarrow Cs^+$ is observed for the FGF. The GF sample completely loses its cesium uptake capacity in presence of sodium excess (seawater for example). Distribution coefficient measurements in radioactive environment with cesium traces confirm the better performance of FGF.

These results demonstrate for the first time the capability to graft $K_2CuFe(CN)_6$ onto a monolithic geopolymer foam and thus withdraw selectively the cesium at trace state in presence of coexisting ions from radioactive liquid waste. Finally our study shows that one gram of this hybrid material is able to efficiently treat 350 liters of cesium contaminated liquid waste.

Acknowledgements

This research was funded by CEA, France. The authors would like to acknowledge Faure Joel and LMAC laboratory (CEA Marcoule) for their assistance with ICP-MS analysis and their contributions to the analytical methods.

Journal Pre-proof

References

- Abousahl, S., Loos-Neskovic, C., Fedoroff, M., 1994. Mechanism of the preparation of insoluble compounds by local growth in aqueous solution. *J. Cryst. Growth* 137, 569–576. [https://doi.org/10.1016/0022-0248\(94\)91000-6](https://doi.org/10.1016/0022-0248(94)91000-6)
- Al-Zboon, K., Al-Harashseh, M.S., Hani, F.B., 2011. Fly ash-based geopolymer for Pb removal from aqueous solution. *J. Hazard. Mater.* 188, 414–421. <https://doi.org/10.1016/j.jhazmat.2011.01.133>
- Ayrault, S., Jimenez, B., Garnier, E., Fedoroff, M., Jones, D.J., Loos-Neskovic, C., 1998. Sorption Mechanisms of Cesium on CuII2FeII(CN)6 and $\text{CuII3[FeIII(CN)6]2}$ Hexacyanoferrates and Their Relation to the Crystalline Structure. *J. Solid State Chem.* 141, 475–485. <https://doi.org/10.1006/jssc.1998.7997>
- Barbosa, V.F.F., MacKenzie, K.J.D., 2003. Synthesis and thermal behaviour of potassium silicate geopolymers. *Mater. Lett.* 57, 1477–1482. [https://doi.org/10.1016/S0167-577X\(02\)01009-1](https://doi.org/10.1016/S0167-577X(02)01009-1)
- Benavent, V., Frizon, F., Poulesquen, A., 2016a. Effect of composition and aging on the porous structure of metakaolin-based geopolymers. *J. Appl. Crystallogr.* 49, 2116–2128. <https://doi.org/10.1107/S1600576716014618>
- Benavent, V., Steins, P., Sobrados, I., Sanz, J., Lambertin, D., Frizon, F., Rossignol, S., Poulesquen, A., 2016b. Impact of aluminum on the structure of geopolymers from the early stages to consolidated material. *Cem. Concr. Res.* 90, 27–35. <https://doi.org/10.1016/j.cemconres.2016.09.009>
- Bortnovsky, O., Dědeček, J., Tvarůžková, Z., Sobalík, Z., Šubrt, J., 2008. Metal Ions as Probes for Characterization of Geopolymer Materials. *J. Am. Ceram. Soc.* 91, 3052–3057. <https://doi.org/10.1111/j.1551-2916.2008.02577.x>
- Chen, C., Wang, J., 2008. Removal of Pb^{2+} , Ag^{+} , Cs^{+} and Sr^{2+} from aqueous solution by brewery's waste biomass. *J. Hazard. Mater.* 151, 65–70. <https://doi.org/10.1016/j.jhazmat.2007.05.046>
- Delchet, C., Tokarev, A., Dumail, X., Toquer, G., Barré, Y., Guari, Y., Guerin, C., Larionova, J., Grandjean, A., 2012. Extraction of radioactive cesium using innovative functionalized porous materials. *RSC Adv.* 2, 5707. <https://doi.org/10.1039/c2ra00012a>
- Duxson, P., Fernández-Jiménez, A., Provis, J.L., Lukey, G.C., Palomo, A., van Deventer, J.S.J., 2007. Geopolymer technology: the current state of the art. *J. Mater. Sci.* 42, 2917–2933. <https://doi.org/10.1007/s10853-006-0637-z>
- El-Naggar, M.R., Amin, M., 2018. Impact of alkali cations on properties of metakaolin and metakaolin/slag geopolymers: Microstructures in relation to sorption of ^{134}Cs radionuclide. *J. Hazard. Mater.* 344, 913–924. <https://doi.org/10.1016/j.jhazmat.2017.11.049>
- Grandjean, A., Barré, Y., Hertz, A., Fremy, V., Mascarade, J., Louradour, E., Prevost, T., 2020. Comparing hexacyanoferrate loaded onto silica, silicotitanate and chabazite sorbents for Cs extraction with a continuous-flow fixed-bed setup: Methods and pitfalls. *Process Saf. Environ. Prot.* 134, 371–380. <https://doi.org/10.1016/j.psep.2019.12.024>
- Haas, P.A., 1993. A Review of Information on Ferrocyanide Solids for Removal of Cesium from Solutions. *Sep. Sci. Technol.* 28, 2479–2506. <https://doi.org/10.1080/01496399308017493>
- Johan, E., Yamada, T., Munthali, M.W., Kabwadza-Corner, P., Aono, H., Matsue, N., 2015. Natural Zeolites as Potential Materials for Decontamination of Radioactive Cesium. *Procedia Environ. Sci.* 28, 52–56. <https://doi.org/10.1016/j.proenv.2015.07.008>
- Lehto, J., Harjula, R., Wallace, J., 1987. Absorption of cesium on potassium cobalt hexacyanoferrate(II). *J. Radioanal. Nucl. Chem. Artic.* 111, 297–304. <https://doi.org/10.1007/BF02072863>
- Lehto, J., Koivula, R., Leinonen, H., Tusa, E., Harjula, R., 2019. Removal of Radionuclides from Fukushima Daiichi Waste Effluents. *Sep. Purif. Rev.* 48, 122–142. <https://doi.org/10.1080/15422119.2018.1549567>

- Liu, P.S., Cui, G., Guo, Y.J., 2016. A lightweight porous ceramic foam loading Prussian blue analogue for removal of toxic ions in water. *Mater. Lett.* 182, 273–276. <https://doi.org/10.1016/j.matlet.2016.07.019>
- Loos-Neskovic, C., Ayrault, S., Badillo, V., Jimenez, B., Garnier, E., Fedoroff, M., Jones, D.J., Merinov, B., 2004. Structure of copper-potassium hexacyanoferrate (II) and sorption mechanisms of cesium. *J. Solid State Chem.* 177, 1817–1828. <https://doi.org/10.1016/j.jssc.2004.01.018>
- Luukkonen, T., Runtti, H., Niskanen, M., Tolonen, E.-T., Sarkkinen, M., Kempainen, K., Rämö, J., Lassi, U., 2016. Simultaneous removal of Ni(II), As(III), and Sb(III) from spiked mine effluent with metakaolin and blast-furnace-slag geopolymers. *J. Environ. Manage.* 166, 579–588. <https://doi.org/10.1016/j.jenvman.2015.11.007>
- Michel, C., Barré, Y., de Dieuleveult, C., Grandjean, A., De Windt, L., 2015. Cs ion exchange by a potassium nickel hexacyanoferrate loaded on a granular support. *Chem. Eng. Sci.* 137, 904–913. <https://doi.org/10.1016/j.ces.2015.07.043>
- Michel, C., Barré, Y., De Windt, L., de Dieuleveult, C., Brackx, E., Grandjean, A., 2017. Ion exchange and structural properties of a new cyanoferrate mesoporous silica material for Cs removal from natural saline waters. *J. Environ. Chem. Eng.* 5, 810–817. <https://doi.org/10.1016/j.jece.2016.12.033>
- Novais, R.M., Ascensão, G., Tobaldi, D.M., Seabra, M.P., Labrincha, J.A., 2018. Biomass fly ash geopolymer monoliths for effective methylene blue removal from wastewaters. *J. Clean. Prod.* 171, 783–794. <https://doi.org/10.1016/j.jclepro.2017.10.078>
- Novais, R.M., Buruberry, L.H., Seabra, M.P., Labrincha, J.A., 2016. Novel porous fly-ash containing geopolymer monoliths for lead adsorption from wastewaters. *J. Hazard. Mater.* 318, 631–640. <https://doi.org/10.1016/j.jhazmat.2016.07.059>
- O'Connor, S.J., MacKenzie, K.J.D., Smith, M.E., Hanna, J.V., 2010. Ion exchange in the charge-balancing sites of aluminosilicate inorganic polymers. *J. Mater. Chem.* 20, 10234. <https://doi.org/10.1039/c0jm01254h>
- Parajuli, D., Takahashi, A., Noguchi, H., Kitajima, A., Tanaka, H., Takasaki, M., Yoshino, K., Kawamoto, T., 2016. Comparative study of the factors associated with the application of metal hexacyanoferrates for environmental Cs decontamination. *Chem. Eng. J.* 283, 1322–1328. <https://doi.org/10.1016/j.cej.2015.08.076>
- Park, Y., Lee, Y.-C., Shin, W.S., Choi, S.-J., 2010. Removal of cobalt, strontium and cesium from radioactive laundry wastewater by ammonium molybdophosphate–polyacrylonitrile (AMP–PAN). *Chem. Eng. J.* 162, 685–695. <https://doi.org/10.1016/j.cej.2010.06.026>
- Petlitzkaia, S., Poulesquen, A., 2019. Design of lightweight metakaolin based geopolymer foamed with hydrogen peroxide. *Ceram. Int.* 45, 1322–1330. <https://doi.org/10.1016/j.ceramint.2018.10.021>
- Sazama, P., Bortnovsky, O., Dědeček, J., Tvarůžková, Z., Sobalík, Z., 2011. Geopolymer based catalysts—New group of catalytic materials. *Catal. Today* 164, 92–99. <https://doi.org/10.1016/j.cattod.2010.09.008>
- Sheha, R.R., Metwally, E., 2007. Equilibrium isotherm modeling of cesium adsorption onto magnetic materials. *J. Hazard. Mater.* 143, 354–361. <https://doi.org/10.1016/j.jhazmat.2006.09.041>
- Skorina, T., 2014. Ion exchange in amorphous alkali-activated aluminosilicates: Potassium based geopolymers. *Appl. Clay Sci.* 87, 205–211. <https://doi.org/10.1016/j.clay.2013.11.003>
- Staunton, S., Roubaud, M., 1997. Adsorption of 137 Cs on montmorillonite and illite; effect of charge compensating cation, ionic strength, concentration of Cs, K and fulvic acid. *Clays Clay Miner.* 45, 251–260.
- Steins, P., Poulesquen, A., Diat, O., Frizon, F., 2012. Structural Evolution during Geopolymerization from an Early Age to Consolidated Material. *Langmuir* 28, 8502–8510. <https://doi.org/10.1021/la300868v>
- Sun, B., Hao, X.-G., Wang, Z.-D., Guan, G.-Q., Zhang, Z.-L., Li, Y.-B., Liu, S.-B., 2012. Separation of low concentration of cesium ion from wastewater by electrochemically switched ion exchange method: Experimental adsorption kinetics analysis. *J. Hazard. Mater.* 233–234, 177–183. <https://doi.org/10.1016/j.jhazmat.2012.07.010>

- Thakur, P., Ballard, S., Nelson, R., 2013. An overview of Fukushima radionuclides measured in the northern hemisphere. *Sci. Total Environ.* 458–460, 577–613. <https://doi.org/10.1016/j.scitotenv.2013.03.105>
- Vincent, T., Vincent, C., Barré, Y., Guari, Y., Le Saout, G., Guibal, E., 2014. Immobilization of metal hexacyanoferrates in chitin beads for cesium sorption: synthesis and characterization. *J. Mater. Chem. A* 2, 10007. <https://doi.org/10.1039/c4ta01128g>
- Vincent, T., Vincent, C., Guibal, E., 2015. Immobilization of Metal Hexacyanoferrate Ion-Exchangers for the Synthesis of Metal Ion Sorbents—A Mini-Review. *Molecules* 20, 20582–20613. <https://doi.org/10.3390/molecules201119718>

Journal Pre-proof

Table captions:*Table 1 : Chemical composition of the fresh water used for the adsorption tests*

Ion	Concentration mol/l
Na ⁺	2.8*10 ⁻⁴
K ⁺	2.6*10 ⁻⁵
Mg ⁺²	1.1*10 ⁻³
Ca ⁺²	2.0*10 ⁻³
Cl ⁻	1.9*10 ⁻⁴
SO ₄ ⁻²	1.3*10 ⁻⁴
HCO ₃ ⁻	5.9*10 ⁻³
NO ₃ ⁻	6.0*10 ⁻⁵
SiO ₂ (aq)	2.5*10 ⁻⁴

*Table 2 : Sodium and potassium concentration released into the solution at equilibrium and cesium sorbed onto the solid (kinetic experiment in deionized water with [Cs⁺]₀ = 7.52*10⁻⁴ mol/l)*

Material	[Na ⁺] released, mol/l	[K ⁺] released, mol/l	[Cs ⁺] sorbed, mol/l	[Na ⁺]/[Cs ⁺]	[K ⁺]/[Cs ⁺]
Geopolymer foams	2.00 10 ⁻³	3.00 10 ⁻⁶	5.6 10 ⁻⁴	3.5	-
Functionalized geopolymer foams	1.00 10 ⁻⁵	7.00 10 ⁻⁴	5,1*10 ⁻⁴	-	1.37

Table 3 : Concentration at equilibrium of sodium and potassium released into the solution and cesium sorbed onto the solid (sorption isotherm in deionized water)

Material	[Na ⁺] released, mol/l	[K ⁺] released, mol/l	[Cs ⁺] sorbed, mol/l	[Na ⁺]/[Cs ⁺]	[K ⁺]/[Cs ⁺]
Geopolymer foams	2.90 10 ⁻³	2.5 10 ⁻⁶	2.00 10 ⁻³	1.45	-
Functionalized geopolymer foams	7.4 10 ⁻⁵	1.3 10 ⁻³	1.3*10 ⁻³	-	1.00

Table 4 : Concentration at equilibrium of sodium and potassium released into the solution and cesium sorbed onto the solid (sorption isotherm in fresh water)

Material	[Na ⁺] released, mol/l	[K ⁺] released, mol/l	[Cs ⁺] sorbed, mol/l	[Na ⁺]/[Cs ⁺]	[K ⁺]/[Cs ⁺]
Geopolymer foams	4.0010^{-3}	$2.00 10^{-6}$	$1.10 10^{-3}$	3.6	-
Functionalized geopolymer foams	$4.00 10^{-5}$	$1.35 10^{-3}$	$8.5*10^{-4}$	-	1.6

Figure captions:

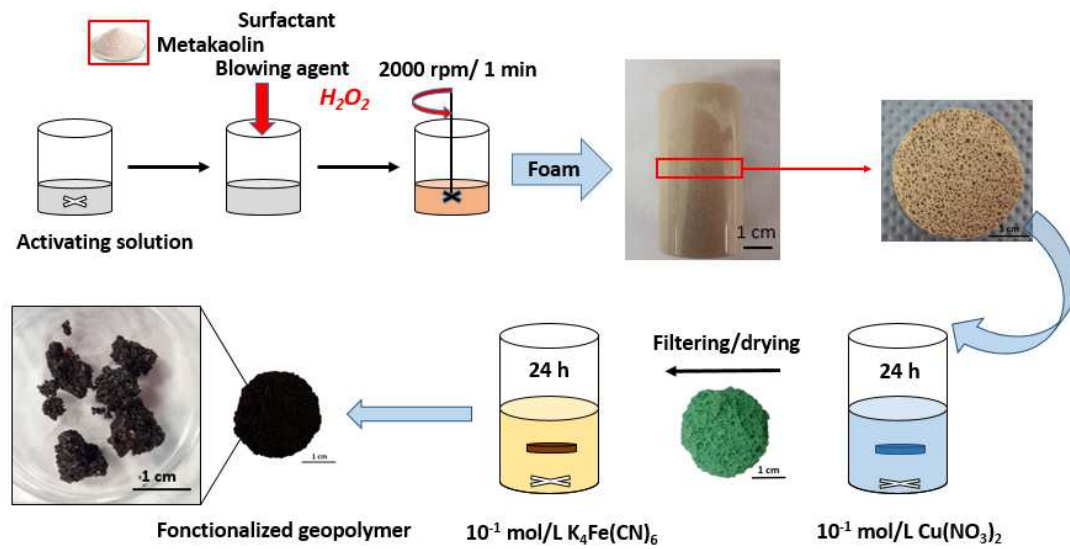
Figure 1: Protocol of synthesis and steps of functionalization of geopolymer foams

Figure 2: SEM images of the functionalized geopolymer foams at various magnifications

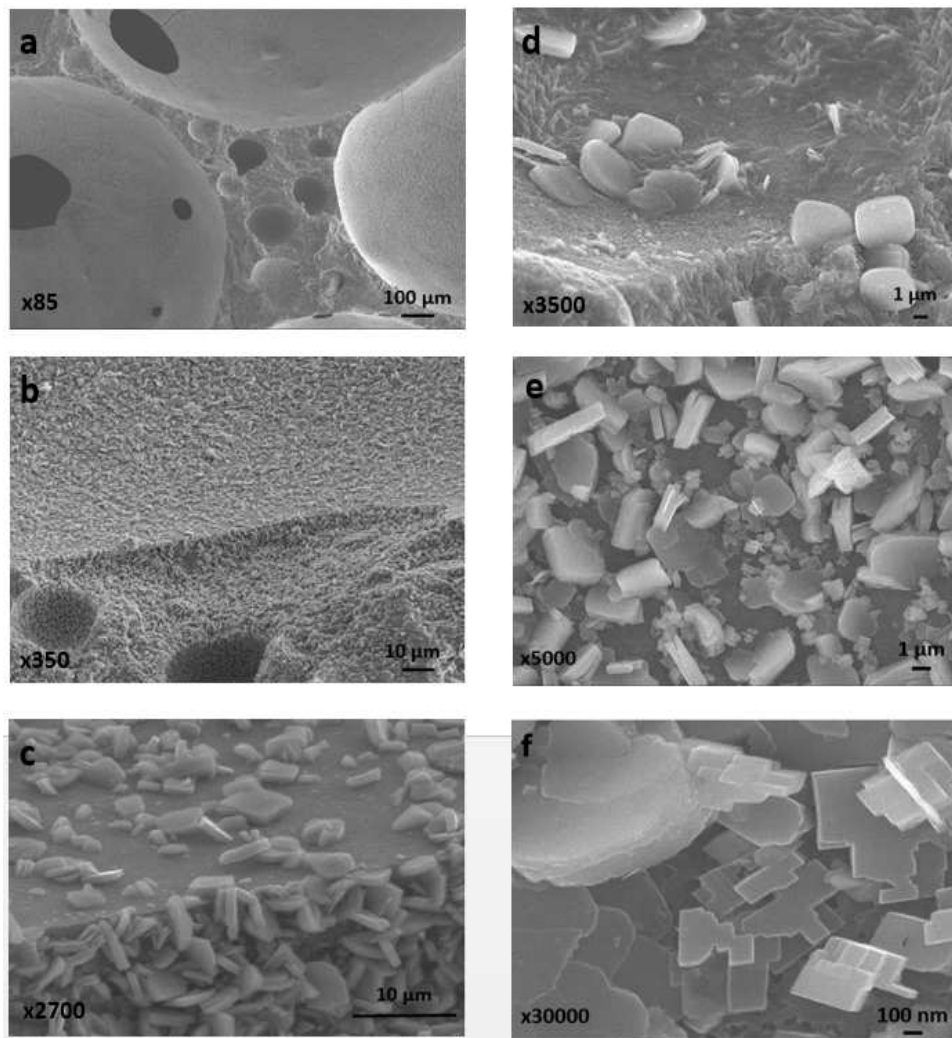


Figure 3 : TEM images and EDX spectra of geopolymer foam before functionalization (a) and after functionalization (b)

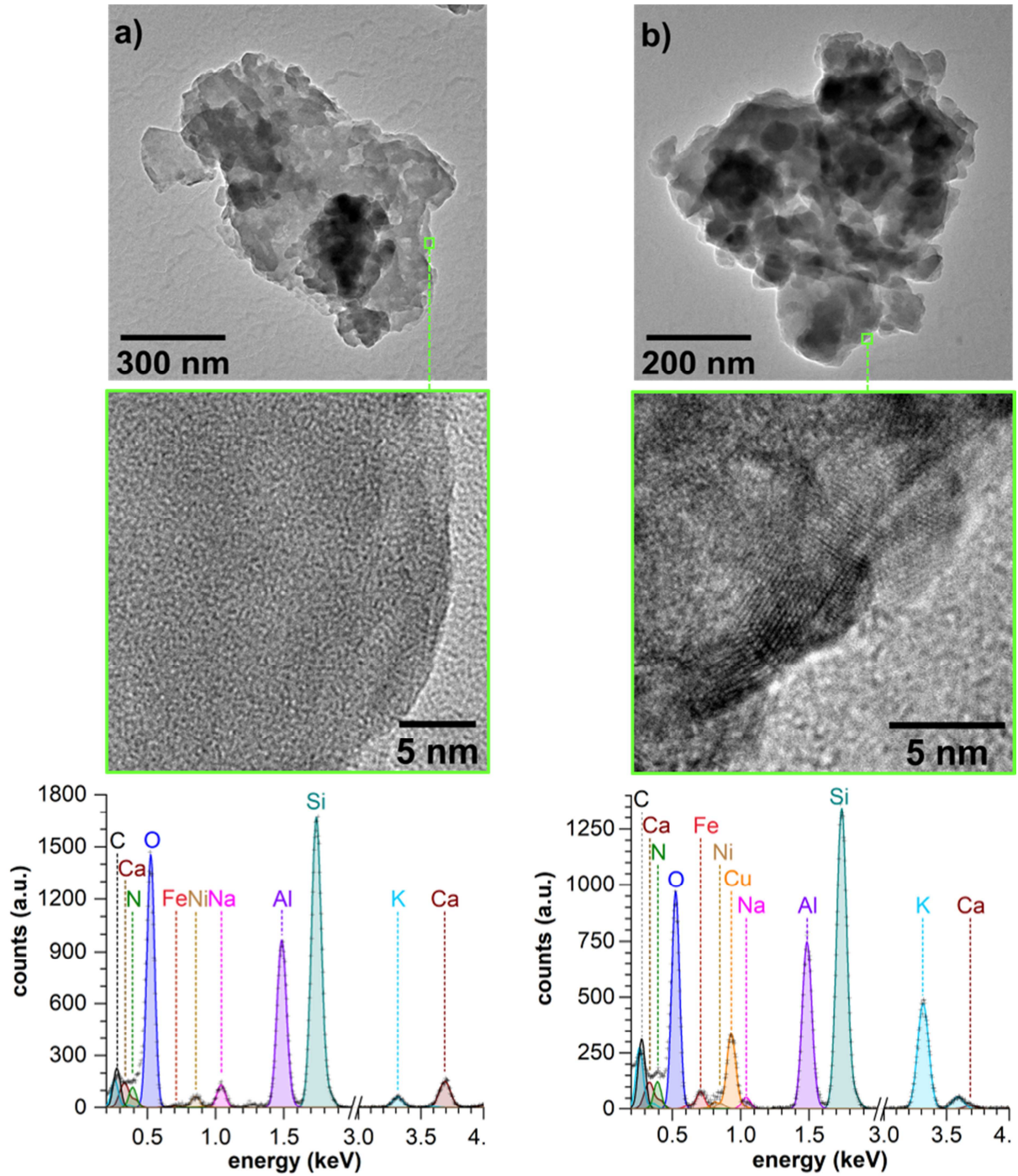


Figure 4 : N₂ adsorption-desorption isotherm for the geopolymer foam and functionalized geopolymer foam

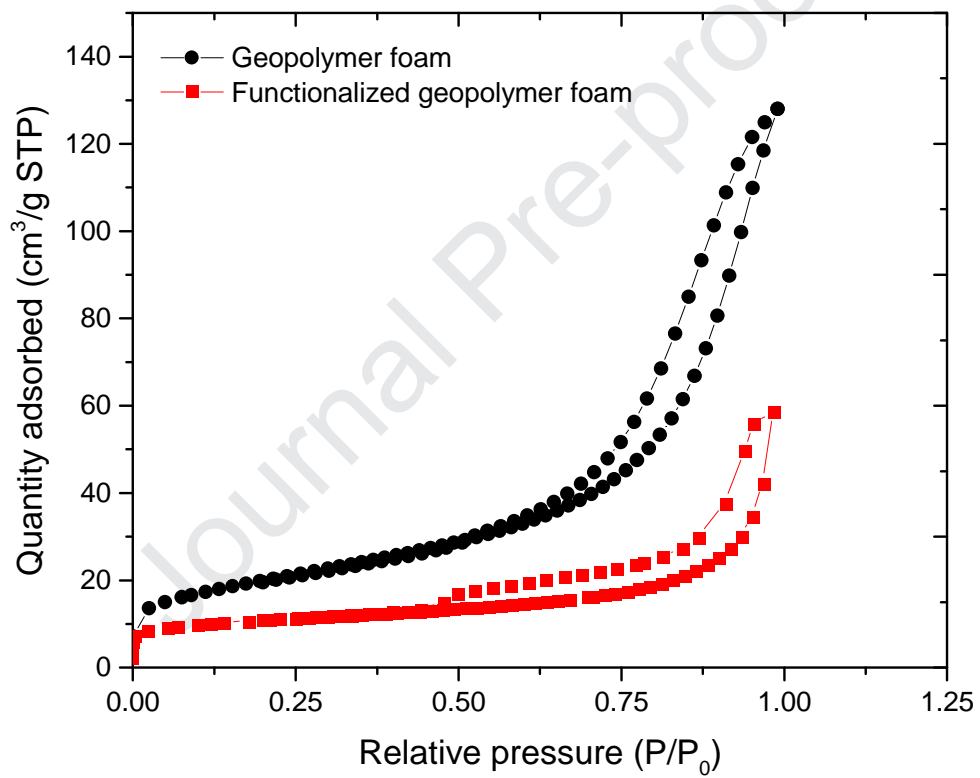


Figure 5: Mineralogical characterization of the geopolymer foam and functionalized geopolymer foam by X-ray diffraction. The FGF pattern was artificially shifted for clarity. The color of atoms for the Rouaite and $K_2Cu(Fe(CN)_6)$ is: Blue for Cu, red for O, light pink for H, grey for N, purple for K, light brown for Fe and dark brown for C. ¹ and ² correspond to 9008310 and 1010372 cif files respectively available in <http://www.crystallography.net/cod/> web site

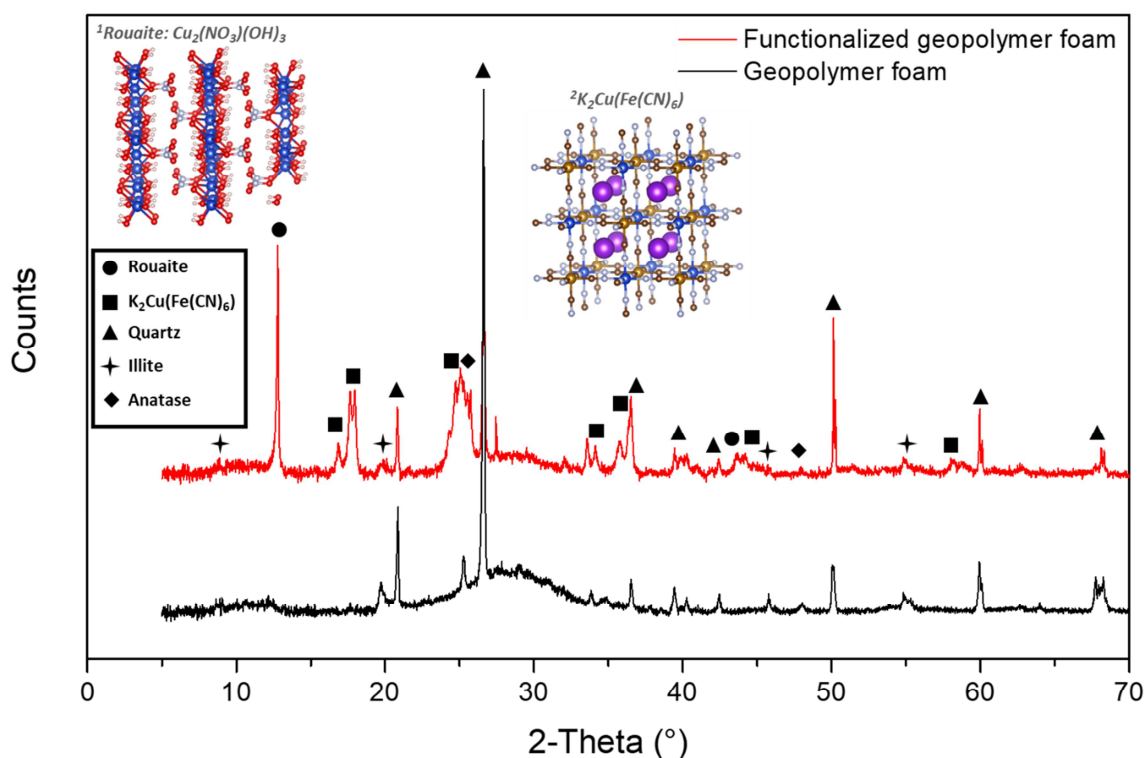


Figure 6: Kinetic of cesium sorption in deionized water on a geopolymer foam and a functionalized geopolymer foam. The initial concentration of cesium is 100 ppm = $7.5 \cdot 10^{-4}$ mol.l⁻¹

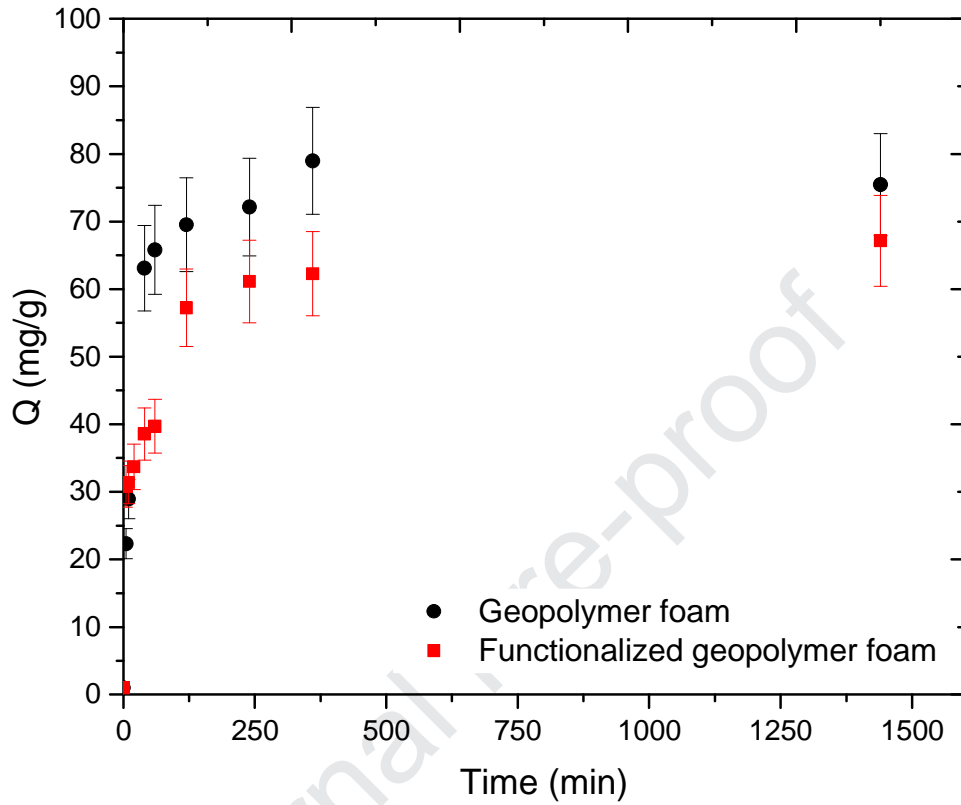


Figure 7: Sorption capacity Q vs C_s concentration in solution for geopolymer foams and functionalized geopolymer foams in deionized water (a) and in fresh water (b)

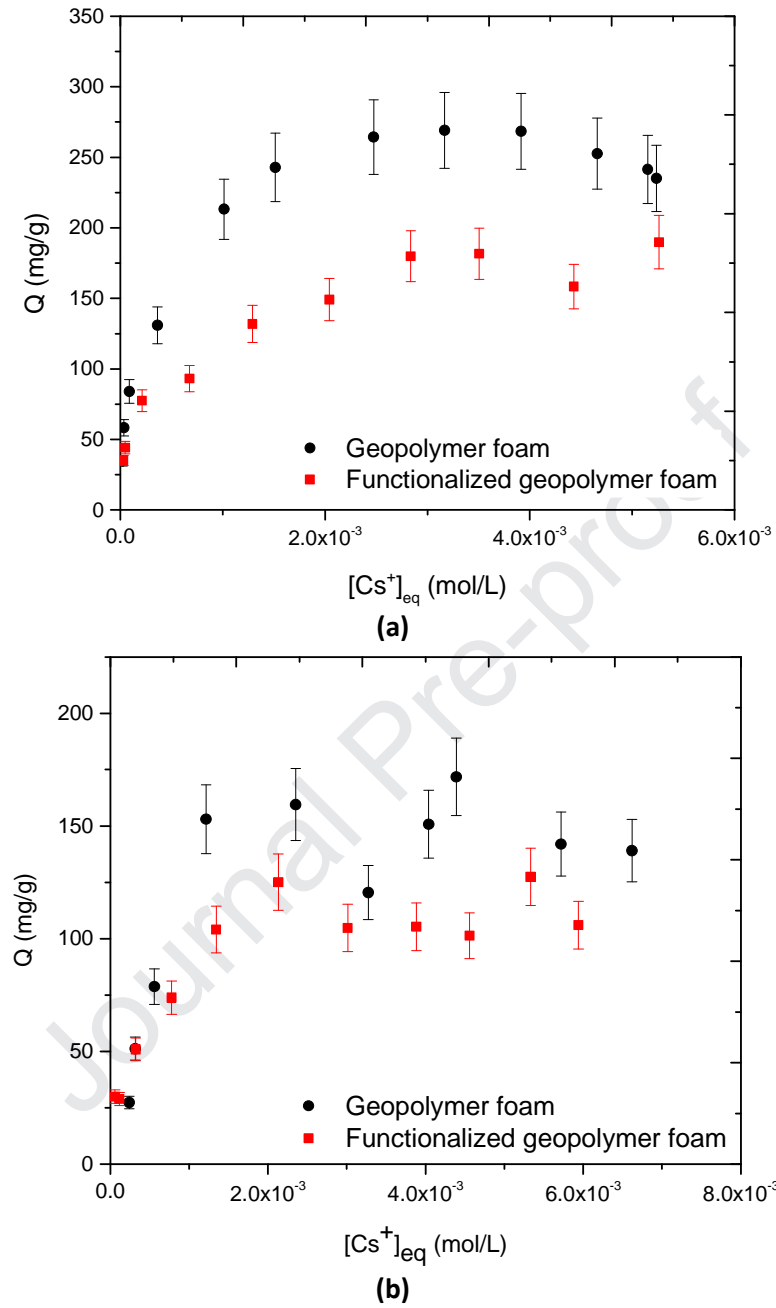


Figure 8: Sorption capacity Q vs Na concentration in solution for geopolymer foams and functionalized geopolymer foams (Fresh water). $[Cs]_0$ was fixed at 50 ppm ($3.76 \cdot 10^{-4}$ mol/L)

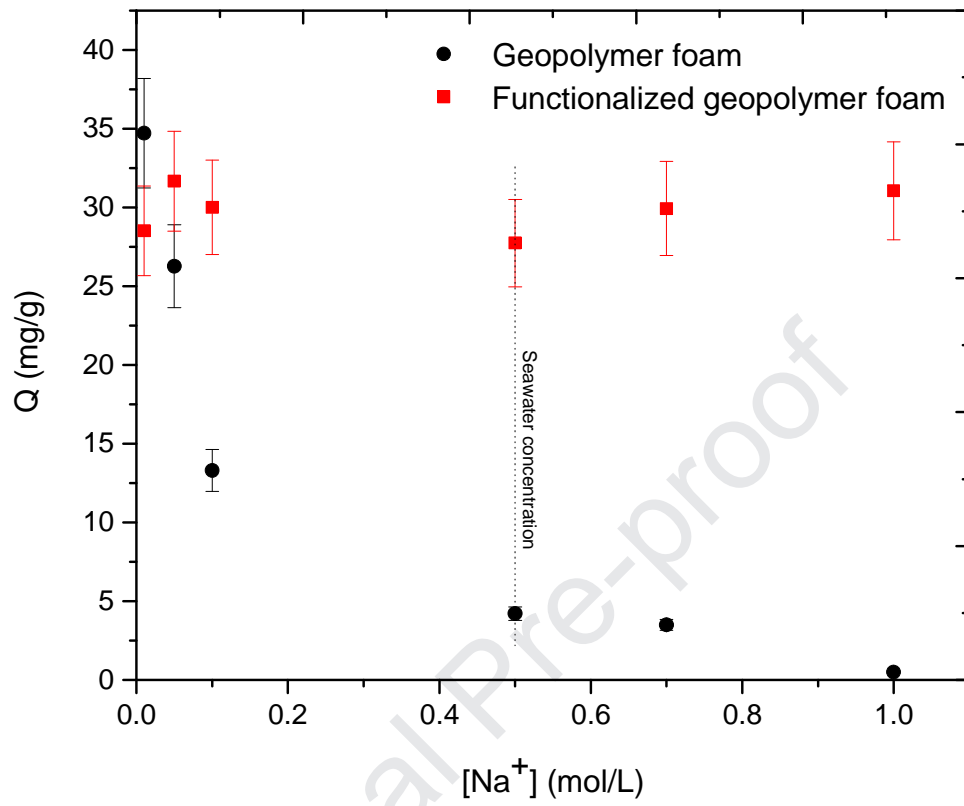
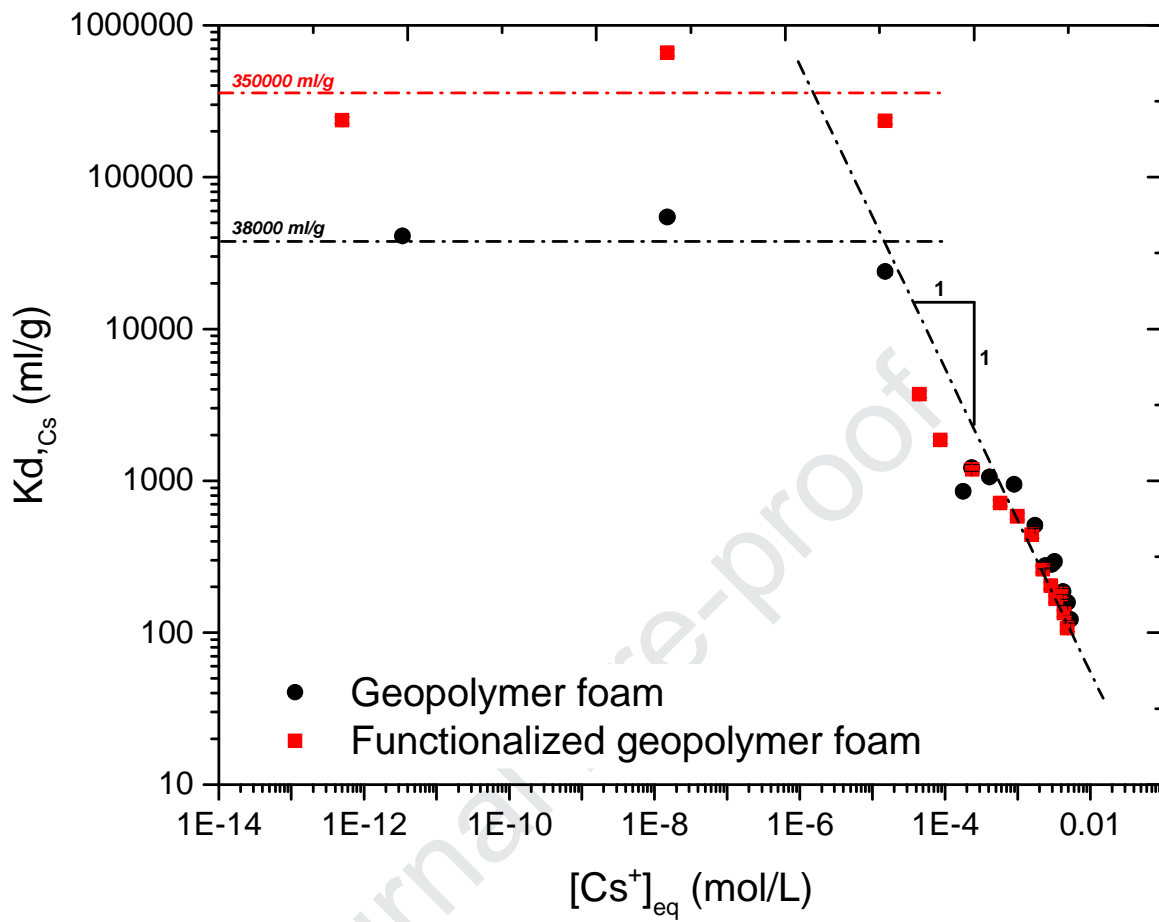


Figure 9: Variation of $K_{d,Cs}$ as a function of $[Cs^+]_{eq}$ for fresh water

Highlights :

- Geopolymer foam with an interconnected pore network functionalized by $[K_2CuFe(CN)_6]$
- FGF decontaminates selectively traces of Cs even in presence of coexisting ions
- GF completely loses its Cs uptake capacity in presence of sodium excess (seawater)
- One gram of FGF is able to efficiently treat 350 liters of Cs contaminated effluent

Declaration of interests

The authors declare that they have no known competing financial interests or personal relationships that could have appeared to influence the work reported in this paper.

The authors declare the following financial interests/personal relationships which may be considered as potential competing interests: